Least Lossy Piezoelectric Energy-Harvesting Charger

Siyu Yang, *Graduate Student Member*, *IEEE*, and Gabriel A. Rincón-Mora, *Fellow*, *IEEE*
School of Electrical and Computer Engineering
Georgia Institute of Technology, Atlanta, USA
Email: jimsyyang@gatech.edu and Rincon-Mora@gatech.edu

***Abstract*—Wireless microsensors can operate indefinitely when they use ambient kinetic energy in motion to replenish the battery. Of available technologies, a switched inductor can draw the most power from a piezoelectric transducer. Power consumption, however, limits how much of that power the battery receives. This paper theorizes and shows that drawing and delivering power with an inductor from the transducer into the battery *directly* reduces the energy the inductor carries. With less energy, inductor current and related ohmic losses are lower. This way, ohmic losses can be up to 74% lower. This is why the switched-inductor bridge is the least lossy piezoelectric charger in the state of the art.**

Keywords—Energy-harvesting charger, switched inductor, direct transfer, least loss, piezoelectric, power supply.

I. Piezoelectric-Powered Chargers

Wireless microsensors embedded in hospitals, factories, cars, and humans can sense, process, and share information that save money, energy, and lives [1]. But since tiny batteries drain quickly, replenishing the battery with ambient power is often necessary [2]. Ambient kinetic energy is a good source because motion is available in many applications [3]–[4].

Reported literature shows that piezoelectric transducers draw, convert, and deliver more power than their electrostatic and electromagnetic counterparts [5]–[13]. Research also shows that switched inductors (SL) draw more power than bridges with fewer power-consuming stages [5]–[8]. These SL chargers essentially collect the charge that the piezoelectric current i_{PZ} in Fig. 1 delivers and that the piezoelectric capacitance C_{PZ} collects.

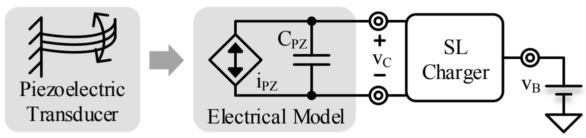

Fig. 1. Piezoelectric-powered energy-harvesting charger.

Unfortunately, series resistance R_{ESR} in the switches and inductor burn some of this energy. So of the energy E_C that C_{PZ} collects across half cycles in Fig. 2 when C_{PZ}'s voltage v_C peaks, the battery receives with E_B what R_{ESR} avails:

$$E_C = 0.5C_{PZ}v_{C(PK)}^2 \tag{1}$$

$$E_B = E_C - E_{LOSS} \tag{2}$$

where E_{LOSS} is the power consumed by the SL. Although CMOS switch resistance R_{SW} is usually less than 100 mΩ, E_{LOSS} is nevertheless significant because inductor resistance R_L in millimeter inductors is normally 1–10 Ω [14].

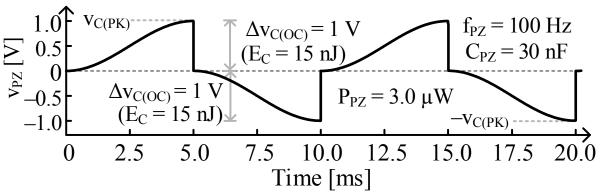

Fig. 2. Piezoelectric voltage in a switched-inductor charger.

This paper theorizes and shows with simulations how to minimize this ohmic loss. Sections II–IV describe and analyze the different ways that a SL can draw and deliver energy from a capacitive source into a battery. Section V then compares and derives which method outputs the most power and identifies which piezoelectric charger in the state of the art is, as a result, the least lossy.

II. Indirect Transfer

A. Switching Configuration

The first configuration of switched-inductor is indirect. The transfer starts with C_{PZ} energizing the inductor L_X, as shown in Fig. 3. When C_{PZ} is completely discharged, L_X with $i_{L(PK)}$ is disconnected to C_{PZ} and instead connected to v_B. Notice that L_X receives all of the energy that from $C_{PZ,}$ and C_{PZ} never directly delivers its energy to the battery.

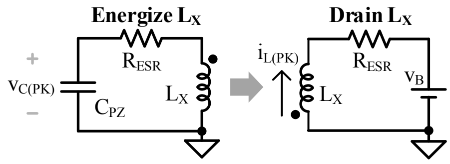

Fig. 3. Inductor phases for indirect transfers.

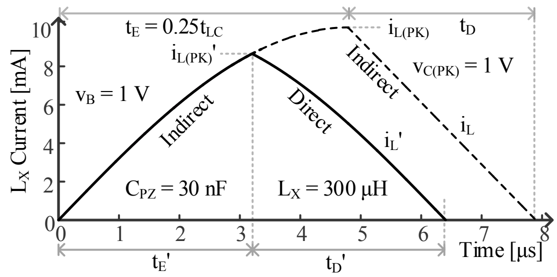

Fig. 4. Inductor current for indirect and indirect–direct transfers.

B. Inductor Current

As shown in the dashed trace in Fig. 4, the energizing part of the transfer is a quarter cycle of the oscillation between C_{PZ} and L_X, as i_L energizes to $i_{L(PK)}$ and v_C discharges to 0:

$$E_L = 0.5L_X i_{L(PK)}^2 \approx E_C, \tag{3}$$

$$i_{L(PK)} \approx \sqrt{\frac{C_{PZ}}{L_X}}v_{C(PK)}. \tag{4}$$

Therefore, the energizing time is a quarter cycle:

$$t_E = 0.25t_{LC} = 0.5\pi\sqrt{L_X C_{PZ}}. \tag{5}$$

Then the inductor drains linearly to the battery with a slope of v_B/L_X, and the draining time is

$$t_D = \left(\frac{L_X}{v_B}\right)i_{L(PK)}. \tag{6}$$

From the current waveform and the transfer time, the ohmic loss of the total series resistance R_{ESR} is

$$E_R = R_{ESR}i_{L(RMS)}^2 t_X = R_{ESR}i_{L(RMS)}^2(t_E + t_D) \tag{7}$$

where $i_{L(RMS)}$ is the root-mean-square (RMS) current across the transfer, and t_X is the total transfer time. A more detailed loss analysis can be found in Section V.

III. Indirect–Direct Transfers

A. Switching Configuration

An alternative way to transfer the energy from C_{PZ} to v_B is the indirect–direct transfer. As shown in Fig. 5, C_{PZ} first energizes L_X, but stops before C_{PZ} is completely drained. Instead, it has drain initial voltage $v_{C(DI)}'$ when L_X starts to drain, and both C_{PZ} and L_X drain directly into the battery to finish the transfer. The controller controls the energizing time so that C_{PZ} and L_X hold just the right amount of energy to drain at the same time at the end of the transfer. C_{PZ} delivers the drain initial energy $E_{C(DI)}'$ directly to the battery, while the rest of the energy, the drain initial energy on the inductor $E_{L(DI)}'$, is delivered indirectly with the inductor. Therefore, it's called indirect–direct transfer.

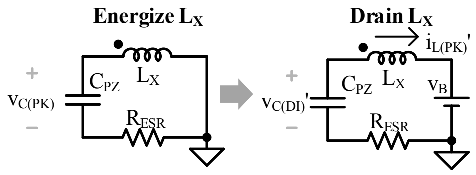

Fig. 5. Inductor phases for indirect–direct transfers.

B. Inductor Current

The inductor current in indirect–direct transfer, i_L' in the solid trace in Fig. 4, starts out the same as in indirect. However, since the energizing time t_E' is shorter, the inductor current only reaches $i_{L(PK)}'$, which is less than $i_{L(PK)}$. Assuming a sinusoidal transfer, the energy between C_{PZ} and L_X before and after t_E' is equal:

$$\begin{aligned} E_C &\approx E_{C(DI)}' + E_{L(DI)}' \\ &= 0.5C_{PZ}v_{C(DI)}'^2 + 0.5L_X i_{L(PK)}'^2 \end{aligned}, \tag{8}$$

where $E_{C(DI)}'$, $E_{L(DI)}'$, $v_{C(DI)}'$, and $i_{L(PK)}'$ denote the drain initial energy on C_{PZ}, the initial energy on L_X, the voltage across C_{PZ}, and the current on L_X at the beginning of the drain phase. The energizing time is the fraction of the cosine that drops the voltage across C_{PZ} from $v_{C(PK)}$ to $v_{C(I)}$,

$$t_E' = \frac{t_{LC}}{2\pi}\cos^{-1}\left(\frac{v_{C(DI)}'}{v_{C(PK)}}\right). \tag{9}$$

Next, both C_{PZ} and L_X drain into v_B across drain time t_D'. Fig. 6 depicts the voltage transfer v_C with the solid line, and the steady-state extrapolation of the oscillation between C_{PZ} and L_X with the dashed trace. The capacitor voltage v_C is a sinusoidal waveform centered around the dc voltage v_{DC} with peaks of $v_{DC} + v_{PK}$ and $v_{DC} - v_{PK}$. In this case, the dc voltage is the battery voltage, v_B, and since the negative peak is 0 V, the peak voltage of the sinusoid, v_{PK}, is v_B. As v_C drains from $v_{C(DI)}'$ to 0, the drain time t_D' is the fraction of the cosine it takes to go from $v_B - v_{C(I)}'$ to v_B,

$$t_D' = \frac{t_{LC}}{2\pi}\cos^{-1}\left(\frac{v_B - v_{C(DI)}'}{v_B}\right). \tag{10}$$

Note that the direct phase of the transfer td' ($0.33t_{LC}$ to $0.50t_{LC}$) in Fig. 6 corresponds with the t_D' in Fig. 4 (3.14 μs to 6.28 μs). Since the voltage is centered at v_B, the energy in the LC tank would need to refer to the dc voltage. When drain phase starts, the inductor has drain initial energy $E_{L(DI)}'$, and C_{PZ} has referred drain initial energy $\Delta E_{C(DI)}'$, which is $E_C - E_{C(DI)}'$ from (8). As the transfer ends, the inductor is drained, so C_{PZ} holds all the energy in the LC tank $\Delta E_{LC}'$. For a sinusoidal transfer, the energy in the LC tank is constant:

$$\begin{aligned} \Delta E_{LC}' = 0.5C_{IN}v_B^2 &\approx \Delta E_{C(DI)}' + E_{L(DI)} \\ &= \Delta E_{C(DI)}' + E_C - E_{C(DI)}' \\ &= 0.5C_{PZ}\left[\left(v_B - v_{C(DI)}'\right)^2 + v_{C(PK)}^2 - v_{C(DI)}'^2\right], \end{aligned} \tag{11}$$

From (11), the exact $v_{C(DI)}'$ to stop energize can be solved for:

$$v_{C(DI)}' = \frac{v_{C(PK)}^2}{2v_B}. \tag{12}$$

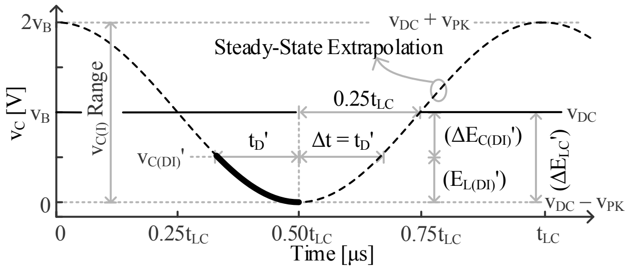

Fig. 6. Steady-state extrapolation of a draining direct transfer.

With $v_{C(DI)}'$, the exact t_E' and t_D' to complete the transfer can be solved for with (9), (10), and (12). Similar to (7), the ohmic loss across an indirect–direct transfer is

$$E_R' = R_{ESR}i_{L(RMS)}'^2 t_X' = R_{ESR}i_{L(RMS)}'^2 (t_E' + t_D'), \tag{13}$$

where $i_{L(RMS)}'$ is the RMS current across this transfer, and t_X' is the total transfer time for indirect-direct. Note that during energize, C_{PZ} drains from $v_{C(PK)}$ to $v_{C(DI)}'$, so $v_{C(DI)}'$ has to be lower than $v_{C(PK)}$. Indirect–direct can only be possible when:

$$v_{C(PK)} \geq v_{C(DI)}' = \frac{v_{C(PK)}^2}{2v_B} \Rightarrow v_{C(PK)} \leq 2v_B. \tag{14}$$

Another way to analyze the condition for indirect–direct is to examine Fig. 6. $v_{C(I)}'$ has a range between ground and the peak of the steady-state extrapolation, $2v_B$,

$$v_{C(DI)}' = \frac{v_{C(PK)}^2}{2v_B} \leq 2v_B \Rightarrow v_{C(PK)} \leq 2v_B. \tag{15}$$

The indirect–direct scheme can draw and deliver more energy than what the inductor carries. Therefore, L_X never receives the entire energy E_C, and the peak inductor current is always lower. The detailed ohmic loss analysis and comparison can be found in Section V.

IV. Direct–Indirect Transfers

A. Switching Configuration

Since indirect–direct transfers only work under certain conditions, another direct configuration is necessary when indirect–direct is not possible. The way to accomplish this is the direct–indirect transfer, where C_{PZ} drains into L_X and v_B to start the transfer, as shown in Fig. 7. Note that v_B has to be lower than $v_{C(PK)}$ for this transfer to start.

As v_C drains from $v_{C(PK)}$ to v_B, L_X energizes. The first phase of the draining L_X has the same switching configuration as the energizing phase, so that both C_{PZ} and L_X can both drain into v_B, until C_{PZ} has no charge. At that point, L_X holds draining current $i_{L(D1)}''$, and is connect to the battery in the second drain phase to complete the transfer. C_{PZ} first delivers part of the energy directly to the battery in energize and drain 1 phase, then the rest of the energy is delivered with the L_X in drain 2 phase. Therefore it's called direct–indirect transfer.

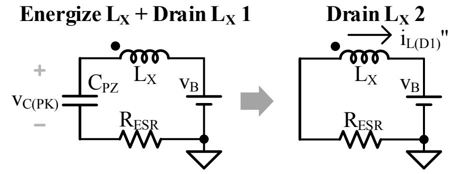

Fig. 7. Inductor phases for direct–indirect transfers.

B. *Inductor Current*

The inductor current i_L'' for direct–indirect is shown in the solid trace in Fig. 8. As a reference, the indirect current i_L is also plotted with the dashed trace. The energizing phase is still a quarter cycle of the LC oscillation,

$$t_E'' = 0.25 t_{LC}. \tag{16}$$

However, since the energizing voltage for L_X is $v_C - v_B$ instead of v_B, the peak current $i_{L(PK)}''$ is lower than $i_{L(PK)}$. The first drain phase continues the L_X oscillation with v_C centered at v_B, and together with the energizing phase make up the direct part of the transfer, as highlighted by the gray region in Fig. 8.

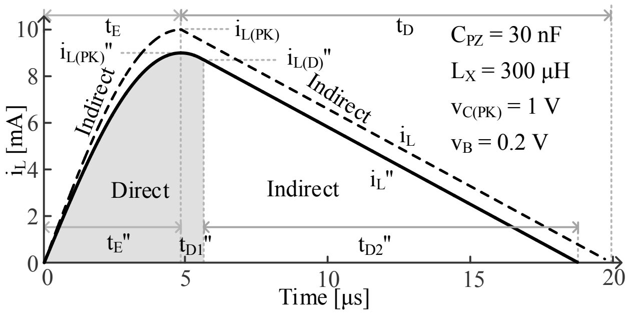

Fig. 8. Inductor current for Indirect-Only and Indirect–Direct transfers.

Figure 9 shows the waveform for v_C and its steady-state extrapolation across the direct phase of the transfer. The steady-state extrapolation is sinusoidal centered at the dc voltage, v_B. Because the v_C starts at $v_{C(PK)}$, the peak voltage of the sinusoidal, v_{PK}, is $v_{C(PK)} - v_B$. The energize phase is a quarter cycle, and the drain 1 phase is a part of quarter cycle. The time it takes for v_C to drain from v_B to 0 is:

$$t_{D1}'' = \frac{t_{LC}}{2\pi} \sin^{-1}\left(\frac{v_B}{v_{C(PK)} - v_B}\right). \tag{17}$$

Because the voltage is centered at v_B, the energy in the LC tank would also need to refer to its dc voltage. At the beginning of the transfer, C_{PZ} hold all the energy in the tank, $\Delta E_{LC}''$. At the end of the direct phase, L_X has drain energy $E_{L(D1)}''$, while C_{PZ} has the referred energy $\Delta E_{C(D1)}''$. Therefore,

$$\begin{aligned}\Delta E_{LC} &= 0.5 C_{PZ} \left(v_{C(PK)} - v_B\right)^2 \\ &\approx \Delta E_{C(D1)}'' + E_{L(D1)}'' \\ &= 0.5 C_{PZ} v_B^{\,2} + 0.5 L_X i_{L(D1)}''^2 \;.\end{aligned} \tag{18}$$

From (18), the drain inductor current is

$$i_{L(D1)}'' = \sqrt{\left(\frac{L_X}{C_{PZ}}\right) v_{C(PK)} \left(v_{C(PK)} - 2v_B\right)}. \tag{19}$$

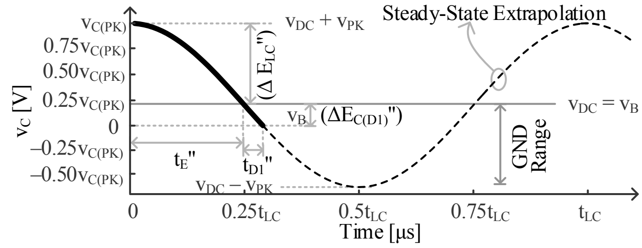

Fig. 9. Steady-state extrapolation of an energizing direct transfer.

The indirect phase of the transfer is between the inductor and the battery, and the inductor current falls linearly. Therefore, the time it takes to drain the inductor is

$$t_{D2}'' = \frac{L_X}{v_B} i_{L(D1)}''. \tag{20}$$

With the transfer time and current profile completed, we can calculate the ohmic loss during a direct–indirect transfer.

$$\begin{aligned}E_R'' &= R_{ESR} i_{L(RMS)}''^2\, t_X'' \\ &= R_{ESR} i_{L(RMS)}''^2\, (t_E'' + t_{D1}'' + t_{D2}''),\end{aligned} \tag{21}$$

where $i_{L(RMS)}''$ is the RMS current across the transfer, and t_X'' is the total transfer time. Direct–indirect draws and delivers more energy than what the inductor carries. Therefore, L_X never receives the entire energy E_C, and the peak inductor current is always lower.

Note from Fig. 9, in order to fully drain C_{PZ} after drain 1, ground has a range between the negative peak of the sinusoid and v_B. Direct–indirect transfer therefore has to satisfy:

$$\begin{aligned}v_{DC} - v_{PK} &= v_B - \left(v_{C(PK)} - v_B\right) \\ &= 2v_B - v_{C(PK)} \le 0 \;,\end{aligned} \tag{22}$$

The same condition can be obtained from (19), since $v_{C(PK)} - 2v_B$ is inside of a square root and therefore has to be non-negative. Interestingly, the condition for direct–indirect transfer complements that for indirect–direct, meaning no matter the relationship between $v_{C(PK)}$ and v_B, we can always choose either direct–indirect or indirect–direct. The only exception is when $v_{C(PK)} = 2v_B$, and that's when both work. In fact, that's the condition when the entire transfer is direct.

V. Comparison and Assessment

Sections II–IV explain how indirect, indirect–direct, and direct–indirect schemes transfer energy. This section discusses how their ohmic losses compare. But since the distinguishing feature is how much energy the inductor carries and both indirect–direct and direct–indirect transfers output more energy than the inductor delivers, this section combines them into one: direct transfers.

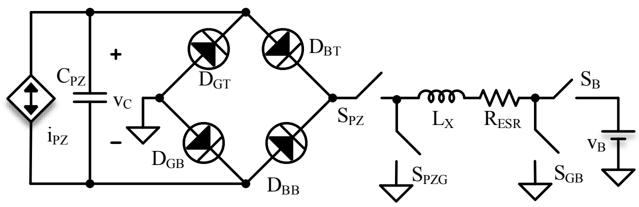

Fig. 10. Bridged switched-inductor charger.

A. CMOS Implementations

The piezoelectric SL charger [7]–[8] in Fig. 10 can perform all three transfers. It's therefore used to simulate the operation and losses for all schemes. Although the switched-inductor bridge [15] in Fig. 11 can only perform direct–indirect transfers, it requires four fewer switches. So Fig. 11 shows the least lossy way of implementing direct transfers.

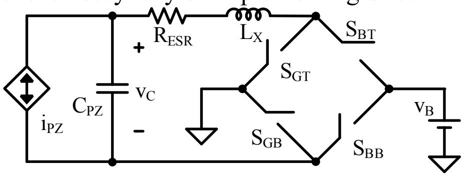

Fig. 11. Switched-inductor bridge.

B. Ohmic Losses

Figure 12 compares the total transfer time and peak current for indirect and direct transfers when $v_{C(PK)}$ is 1 V and v_B is between 0.1 and 5 V. The direct–indirect region (where v_B is less than 0.5 V) is in grey and the indirect–direct region is not. The y-axis indicates the fraction of time t_X' and t_X'' and peak current $i_{L(PK)}'$ and $i_{L(PK)}''$ that direct transfers require relative to indirect transfers t_X and $i_{L(PK)}$. This means that $i_{L(PK)}'$, for example, nearly matches $i_{L(PK)}$ when v_B is 5 V.

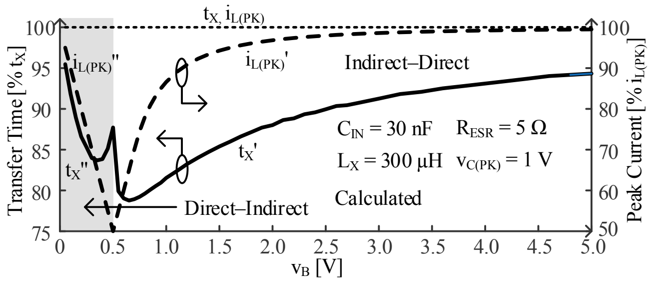

Fig. 12. Transfer times and peak currents for indirect and direct transfers.

As simulation results show, direct transfers t_X' and t_X'' require 80%–95% of the time that indirect transfers require with t_X. Plus, peak currents $i_{L(PK)}'$ and $i_{L(PK)}''$ for direct transfers are 50%–98% of the $i_{L(PK)}$ that for indirect transfers. With shorter transfers and lower currents, R_{ESR} consumes less ohmic power with direct transfers than with indirect.

Figure 13 shows ohmic losses for indirect and direct transfers. The y-axis here indicates the fraction of power that R_{ESR} loses with direct transfers E_R' and E_R'' relative to indirect transfers E_R when v_B is 0.1–5 V. As shown, direct transfers burn 26%–86% of the power that indirect transfers consume with the same 5 Ω. Simulation validates the theory, as shown by the gray dashed traces in Fig. 13. The maximum error is 8% for indirect transfer, and 6% for direct transfers.

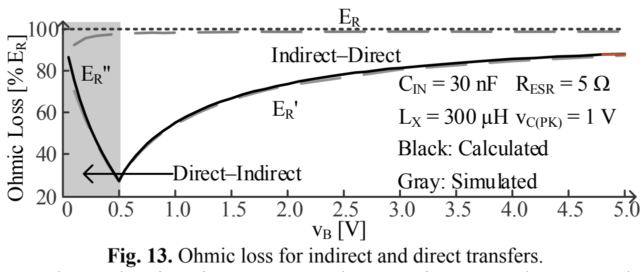

Fig. 13. Ohmic loss for indirect and direct transfers.

The reduction is greatest when v_B is 0.5 V because the inductor energizes and drains with direct transfers. So although transfer time (t_X' and t_X'') is not the shortest, peak inductor current $i_{L(PK)}'$ and $i_{L(PK)}''$ is so low that R_{ESR} still burns the least power. In other words, the loss is lower when more of the transfer is direct. This is why the switched-inductor bridge in Fig. 11 is the least lossy in the state of the art, because it transfers more power directly than the others.

VI. Conclusions

The switched-inductor bridge is the least lossy piezoelectric charger in the state-of-the-art because of low ohmic loss. Utilizing direct transfers, the inductor can draw and deliver more energy than it carries. As a result, both transfer time and peak inductor current are reduced, and the related ohmic loss is reduced by as much as 74%. With direct transfers, more power from piezoelectric transducers that draws from ambient motion can reach the battery. This battery can therefore indefinitely power the wireless microsensors to save energy, money, and lives.

Acknoledgment

The authors thank Dr. Lazaro, Dr. Blanco, Dr. Morroni, and Texas Instruments for their sponsorship and support.

References

[1] D. Puccinelli and M. Haenggi, "Wireless sensor networks: applications and challenges of ubiquitous sensing," *IEEE Circuits and Syst. Mag.*, vol. 3, no. 3, pp. 19–29, 2005.

[2] S.P. Beeby, M.J. Tudor, and N.M. White, "Energy harvesting vibration sources for micro-systems applications," *Measurement Science and Technology*, vol. 17, no. 12, pp. 175–195, Oct. 2006

[3] S. Suduvalayam and P. Kulkarni, "Energy harvesting sensor nodes: Survey and implications," *IEEE Commun. Surveys Tut.*, vol. 13, no. 3, pp. 443–543 461, Jul.–Sep. 2011.

[4] S. Roundy, P.K. Wright, and J. Rabaey, "A study of low level vibrations as a power source for wireless sensor nodes," *Comput. Commun.*, vol. 26, no. 11, pp. 1131–1144, Jul. 2003.

[5] D. Kwon and G.A. Rincón-Mora, "A single-inductor 0.35-µm CMOS energy-investing piezoelectric harvester," *IEEE J. of Solid-State Circuits*, vol. 49, no. 10. pp. 2277–2291, Oct. 2014.

[6] D. Kwon and G.A. Rincón-Mora, "A 2-um BiCMOS rectifier-free ac-dc piezoelectric energy harvester-charger IC," *IEEE Trans. Biomedical Circuits Systems*, vol. 4, no. 6. pp. 400–409, Dec. 2010.

[7] G. Ottman, H.F. Hofmann, A.C. Bhatt, and G.A. Lesieutre, "Adaptive piezo-electric energy harvesting circuit for wireless remote power supply," *IEEE Trans. on Power Electronics*, vol. 17, no. 5, pp. 669–676, May 2002.

[8] G.A. Rincón-Mora and S. Yang, "Tiny piezoelectric harvesters: Principles, constraints, and power conversion," *IEEE Trans. on Circuits Syst. I*, vol. 63, no. 5, pp. 639–649, May 2016.

[9] J. Dicken, P.D. Mitcheson, I. Stoianov, and E.M. Yeatman, "Power-Extraction Circuits for Piezoelectric Energy Harvesters in Miniature andLow-Power Applications," *IEEE Trans. on Power Electronics*, vol. 27,no. 11, pp. 4514–4529, Nov. 2012

[10] Y.K. Ramadass and A.P. Chandrakasan, "An efficient piezoelectric energy harvesting interface circuit using a bias-flip rectifier and shared inductor," *IEEE J. of Solid-State Circuits*, vol. 45, no. 1, pp. 189–204, Jan. 2010.

[11] Y.C. Chu, I. C. Lien, and W.J. Wu, "An improved analysis of the SSHI interface in piezoelectric energy harvesting," *Smart Mater. Struct.*, vol. 16, no. 6, pp. 2253–2264, Oct. 2007.

[12] P.D. Mitcheson, T.C. Green, and E.M Yeatman, "Power processing circuits for electromagnetic, electrostatic and piezoelectric inertial energy scavengers," *Microsyst. Technol.*, vol. 13, no. 11, pp. 1629–1635, Jul. 2007.

[13] K. Yoon, S.W. Hong, and G.H. Cho, "Double pile-up resonance energy harvesting circuit for piezoelectric and thermoelectric materials," *IEEE J. of Solid-State Circuits*, vol. 53, no. 44, pp. 1049–1060, Apr. 2018.

[14] R.D. Prabha and G.A. Rincón-Mora, "Maximizing Power-Transfer Efficiency in Low-Power DC-DC Converters," *IET Electronic Letters*, vol. 51, no. 23, pp. 1918–1920, Nov. 2015.

[15] S. Yang and G.A. Rincón-Mora, "Energy-harvesting piezoelectric-powered CMOS series switched-inductor bridge", *IEEE Trans. on Power Electronics*, 2018 (Early Access).